Title

Design and evaluation of a device for fast multispectral time-resolved fluorescence spectroscopy and imaging.

Permalink

https://escholarship.org/uc/item/60x0c765

Journal

The Review of scientific instruments, 85(3)

ISSN

0034-6748

Authors

Yankelevich, Diego R
Ma, Dinglong
Liu, Jing
et al.

Publication Date

2014-03-01

DOI

10.1063/1.4869037

Peer reviewed

CrossMark
click for updates

Design and evaluation of a device for fast multispectral time-resolved fluorescence spectroscopy and imaging

Diego R. Yankelevich,[1,2] Dinglong Ma,[2] Jing Liu,[2] Yang Sun,[2] Yinghua Sun,[2] Julien Bec,[2] Daniel S. Elson,[3] and Laura Marcu[2,a)]

[1]*Department of Electrical and Computer Engineering, University of California, 3101 Kemper Hall, Davis, California 95616, USA*
[2]*Department of Biomedical Engineering, University of California, 451 Health Sciences Drive, Davis, California 95616, USA*
[3]*Hamlyn Centre for Robotic Surgery, Department of Surgery and Cancer, Imperial College London, Exhibition Road, London SW7 2AZ, United Kingdom*

The application of time-resolved fluorescence spectroscopy (TRFS) to *in vivo* tissue diagnosis requires a method for fast acquisition of fluorescence decay profiles in multiple spectral bands. This study focusses on development of a clinically compatible fiber-optic based multispectral TRFS (ms-TRFS) system together with validation of its accuracy and precision for fluorescence lifetime measurements. It also presents the expansion of this technique into an imaging spectroscopy method. A tandem array of dichroic beamsplitters and filters was used to record TRFS decay profiles at four distinct spectral bands where biological tissue typically presents fluorescence emission maxima, namely, 390, 452, 542, and 629 nm. Each emission channel was temporally separated by using transmission delays through 200 μm diameter multimode optical fibers of 1, 10, 19, and 28 m lengths. A Laguerre-expansion deconvolution algorithm was used to compensate for modal dispersion inherent to large diameter optical fibers and the finite bandwidth of detectors and digitizers. The system was found to be highly efficient and fast requiring a few nano-Joule of laser pulse energy and <1 ms per point measurement, respectively, for the detection of tissue autofluorescent components. Organic and biological chromophores with lifetimes that spanned a 0.8–7 ns range were used for system validation, and the measured lifetimes from the organic fluorophores deviated by less than 10% from values reported in the literature. Multi-spectral lifetime images of organic dye solutions contained in glass capillary tubes were recorded by raster scanning the single fiber probe in a 2D plane to validate the system as an imaging tool. The lifetime measurement variability was measured indicating that the system provides reproducible results with a standard deviation smaller than 50 ps. The ms-TRFS is a compact apparatus that makes possible the fast, accurate, and precise multispectral time-resolved fluorescence lifetime measurements of low quantum efficiency sub-nanosecond fluorophores. © *2014 AIP Publishing LLC*. [http://dx.doi.org/10.1063/1.4869037]

I. INTRODUCTION

Fluorescence spectroscopy is a powerful technique for *in vivo* tissue diagnosis. Of particular interest for clinical applications, time- and wavelength-resolved fluorescence spectroscopy has proven to be a reliable technique for tissue characterization as is capable of providing multiple parameters including fluorescence intensity, spectrum, and lifetime.[1–4] Moreover, time-resolved fluorescence spectroscopy can improve the specificity of fluorescence measurements as such measurements are virtually independent of fluorescence intensity. Conditions that typically hamper steady-state fluorescence measurements such as the non-uniform tissue illumination due to irregularities at the tissue surface, the variation of fluorescence intensity due to changes in fluorescence excitation-collection geometries, or the attenuation of spectral intensity due the presence of endogenous absorbers (e.g., blood) have a minor effect on the excited state lifetimes.[4–7]

Multiple endogenous fluorophores in tissue (e.g., structural proteins, enzyme co-factors, porphyrins, and lipoproteins) can be excited simultaneously by a single wavelength. Subsequently, the measured tissue fluorescence emission represents a superposition of many spectrally overlapping fluorescent molecules, which results in a variation of fluorescence lifetime with wavelength. Thus, for a more effective use of fluorescence lifetime(s) information, measurements of spectrally resolved fluorescence decay characteristics are required. For tissue diagnosis, this has typically been achieved through the use of either a scanning monochromator[1,8] or a set of band-pass filters[3,9] that can resolve the sample emission spectrum sequentially before each spectral intensity is time-resolved. The common methods for resolving the emission decay characteristics include time-correlated single photon counting (TCSPC),[10,11] time-gated,[12,13] and pulse sampling.[3,14] However, recording of fluorescence decays at multiple wavelengths is inherently associated with long data

---

a)Author to whom correspondence should be addressed. Electronic mail: lmarcu@ucdavis.edu

acquisition time that limits the applicability of this technique to static measurements.

To overcome this problem, a multi-detector scheme for TCSPC has been extended to the simultaneous detection at several emission spectral channels where histograms depicting the probability of photons arrival time for all wavelengths are built-up simultaneously.[10,15] However, this scheme can be very costly if sub-nanosecond detectors are used. It also requires multiple high voltage sources that considerably complicate the system. Moreover, to avoid photon pile-up the count rate needs to be reduced to 1%–5% of the excitation rate.[16]

An alternative solution for simultaneous recording of fluorescence decays in multiple spectral bands was recently reported by our group.[9] In this earlier configuration, the emission spectrum was resolved using a set of dichroic and bandpass filters allowing for selection of three channels or wavelength bands. Each channel was coupled to optical fibers of different lengths which acted as optical delay lines. Consequently the spectrally resolved fluorescence pulses arrived at the detector separated in time (∼50 ns). The time-resolved spectroscopic technique is based on a pulse sampling and gated detection where the detector is kept on until the entire fluorescence transient pulse is detected. This pulse is sampled using a digitizer with high sampling frequency and analog bandwidth. If the sample has high quantum efficiency, a single excitation pulse is enough to simultaneously record a complete transient fluorescent pulse for each channel (wavelength band). This method allows fast recording (∼few microseconds) of fluorescence decays in multiple spectral bands generated in response to a single excitation event. Moreover, the exposure to a reduced number of optical pulses, and hence low average optical power, minimizes the effect of photobleaching on the measurement.

While this initial prototype demonstrated the ability to analyze the biochemical features of diverse tissues, and to retrieve robust time-resolved data during tissue scanning,[17] the practical implementation of the concept was hampered by the use of a low repetition-rate electrical discharge nitrogen laser source. This pulsed light source has been most commonly used for inducing single-photon tissue autofluorescence in time-resolved pulse sampling techniques schemes. Although the nitrogen laser emits highly energetic microjoule pulses, the typical repetition rate is only tens of Hertz, with long pulse widths (approaching 1 ns) and poor pulse amplitude stability. These factors limit the data acquisition rate, temporal resolution and storage speed as well as the scanning speed when making multiple measurements in series. In addition, this prototype used a relatively expensive, fragile, and bulky digitizing oscilloscope for data acquisition, was difficult to expand to other wavelengths of biological interest, and had large footprint.

In this article, we report a fast multispectral time-resolved fluorescence spectroscopy (ms-TRFS) system designed to address the limitations of the early prototype.[9] In addition, we present for the first time the theoretical and practical aspects pertaining to the evaluation of such ms-TRFS device and evaluated its performance. The new system enables high speed of data acquisition (e.g., <1 μs per data point from four spectral channels) and has enhanced portability, thus is highly compatible with measurements in clinical environment. In addition, the current system enables fluorescence data acquisition/analysis protocols in multiple operation modes in four spectral channels: point-spectroscopy, line-scanning, and planar XY-scanning which enables recovery of a spectroscopic image or fluorescence lifetime imaging (FLIm). The spectral channels can be adapted to resolve the autofluorescence emission of key biomolecules in tissue (e.g., collagen, nicotinamide adenine dinucleotide (NADH), elastin, lipopigments, flavins, and porphyrins). The apparatus behind this ms-TRFS system takes advantage of recent advances in optoelectronic devices that improve the performance of pulse sampling and gated detection technique. The ability of this system to robustly operate via long multimode optical fibers and to accurately resolve the fluorescence lifetimes is also reported.

II. MATERIALS AND METHODS

The schematic diagram of the ms-TRFS system, which includes the main opto-mechanical components, is shown in Figure 1. Its foremost components are a fluorescence excitation source, a compact wavelength-selection-module and a fast-response fluorescence detector and portable digitizer. A detailed description of each component follows.

A. Laser source and configuration of the fluorescence excitation-collection

The excitation source is a compact and robust diode-pumped modelocked Ytterbium fiber laser (Fianium UVPower355-0.2-PP-CST) which emits pulses at 355 nm, 30 ps pulse width, 60 nJ energy per pulse at 1 MHz repetition rate. The schematic diagram of the fTRFS experimental configuration and a photograph of the wavelength-selection-module are shown in Fig. 1. The delivery of the excitation light was implemented with a 600 μm core diameter, 0.22 NA, 3.2 m long fiber (Polymicro FVP600660710). The laser pulses were collimated with a 6 mm diameter, 10 mm focal length UV-coated fused silica lens (Thorlabs LA4280-UV) and directed to the fiber port by a dichroic beam-splitter (BS1 in Fig. 1(a)) with >99% reflectance for 340–360 nm and >93% transmittance for 360–800 nm wavelengths (Chroma Technologies z355rdc). The collection of the sample florescence pulses was also performed by the same excitation fiber which delivered them back to the wavelength-selection-module.

B. Wavelength selection module

The wavelength selection module consisted of a tandem array of 45° dichroic beamsplitters, bandpass filters and optical fiber ports, or optical channels (Fig. 1). Six fiber ports (that coupled light from free space into the optical fibers and vice versa) completed the system: a port for the delivery of UV laser pulses into the instrument, a port used in bidirectional mode for sample excitation and fluorescence pulse detection and four ports to sort the fluorescence pulses into
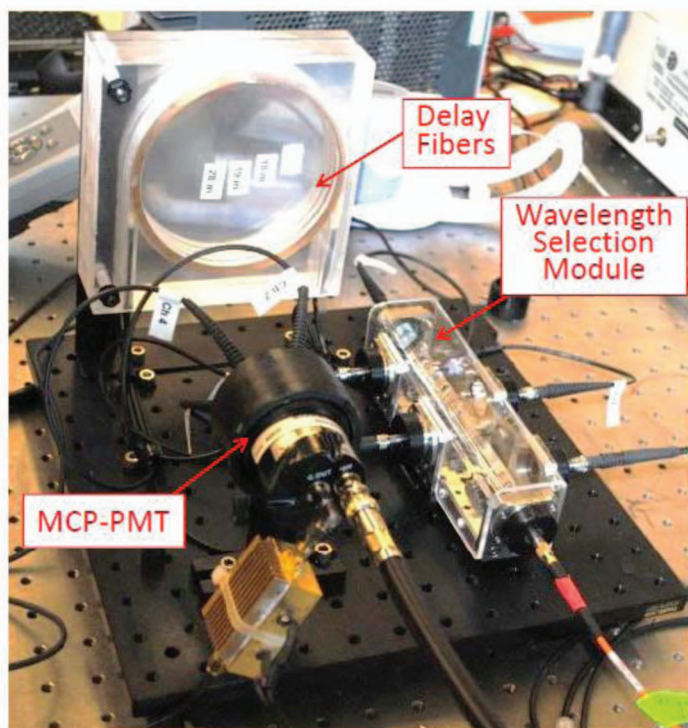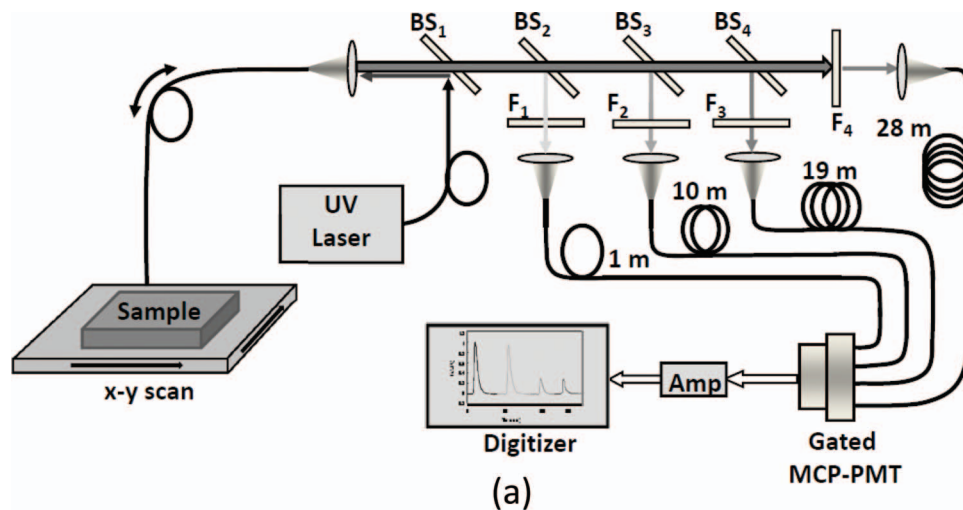
FIG. 1. (a) Schematic diagram of the ms-TRFS experimental configuration. F_1–F_4 are optical pass-band filters with center wavelength/bandwidth: 390/40, 452/45, 542/50, and 629/53 nm, respectively. BS_1–BS_4 are dichroic beam-splitters with >93% transmittance for wavelengths longer than 360, 420, 510, and 590 nm, respectively. (b) Photograph of wavelength-selection-module, multimode fiber optic delay lines, and fluorescence detection components. All the components of the fiber selection module are mounted on a compact 36 × 165 mm breadboard.

optical channels with clinically relevant passband wavelengths. All fiber optic ports consisted of vertical plates (Thorlabs HCA3-SM1), with a one inch aperture with SM1 inner thread, attached to the sides of the breadboard. The system was constructed on a compact stainless steel "fiber-bench" breadboard (Thorlabs FT-38×165) with 36 × 165 mm dimensions. All dichroic beamsplitters were cut to 9 × 9 mm size and glued to a flexure mounting table base with 45° orientation with respect to the optical ports (Thorlabs ACBV). The mounting table allowed precise adjustment of tip, tilt, and rotation of each dichroic. The dichroic beamsplitters BS2-4 had >93% transmittance for wavelengths longer than

420 nm (Semrock Di01-R405-25×36), 510 nm (Semrock FF510-Di01-25×36) and 590 nm (Semrock FF593-Di02-25×36), respectively.

The bandpass filters, mounted in the vertical fiber port plates, had center wavelengths/bandwidths of 390/40 nm (F1: Semrock FF01-390/40-25), 452/45 nm (F2: FF01-452/45-25), 542 nm/50 nm (F3: FF01-542/50-25), and 629/53 nm (F4: FF01-629/53-25). A compact fiber micro-positioner with six directional adjustments (Thorlabs PAF-SMA-11A) was also attached to the vertical port plates enabling coupling to SMA-terminated fibers. Coupling of the filtered fluorescence into the optical fibers was achieved with 6 mm diameter,

10 mm focal length fused silica lenses (Thorlabs LA4280). The fluorescence pulses, now sorted by wavelength into each optical channel, were time-delayed by ~44 ns with four SMA terminated 200 μm diameter, 0.22 NA, step-index multimode optical fibers (Polymicro FVP2000220240) with 1, 10, 19, and 28 m length, the shortest wavelength channel having the smallest delay. The different length optical fibers were coiled in a compact spool constructed from plexiglass plates and connected to a single detector. The wavelength selection module, detector, and fiber spools were mounted on a 30 × 30 cm breadboard for portability.

C. Characterization of the wavelength selection module throughput

The characterization of the optical throughput of all channels was performed using a Xenon lamp (Photon Technologies International PowerArc), emitting photons that spanned from the UV to IR, coupled to a multimode optical fiber. The broadband optical radiation was directed to all channels by connecting the fiber to the sampling port of the wavelength selection module (see Fig. 1). The spectra transmitted by each optical channel were measured using a compact CCD array spectrometer (Ocean Optics USB2000). Given that the spectral response of the spectrometer and Xe lamp were not flat, normalization was performed with a spectral scan taken by connecting the fiber coupled to the Xe lamp directly to the spectrometer. The normalized optical throughput, measured after optimizing the alignment of each channel, is shown in Fig. 2.

D. Time-resolved fluorescence detection

The detection of the fluorescence emission was performed with a multichannel plate (MCP) gated intensified PMT (Hamamatsu R5916U-50) with a 350 ps FWHM re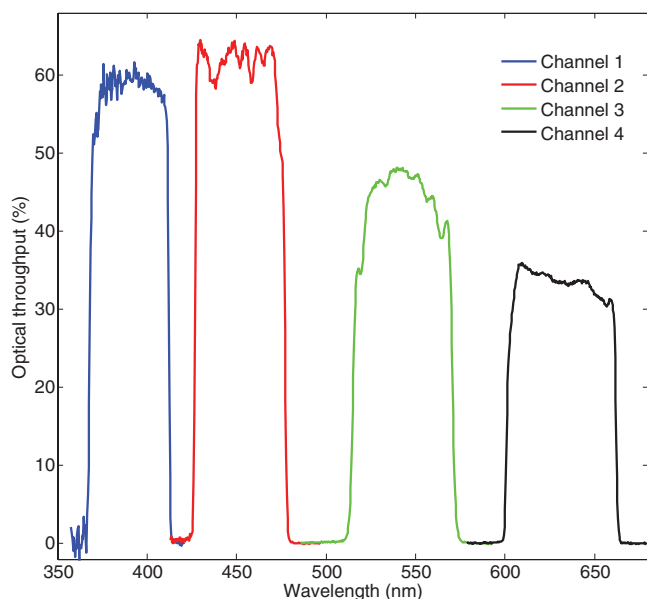sponse time powered by a 0–3000 V supply (Ortec 556) and gated with a 1 μs, 40 V pulse. In this article "gated" means that the PMT is only active during the time period where the fluorescence decay is expected and does not refer to sampling of the fluorescence decay using ultrashort gates, as in other fluorescence lifetime imaging microscopy (FLIM) detection methods.[12, 18, 19] The fluorescence pulses are time delayed by an amount that depends on the channel that matches their emission spectra and directed to the MCP-PMT in a configuration that ensures balanced detection from all optical channels with minimal loss. The distal fiber ends were attached onto a custom-made adapter with four SMA connectors that orient the fiber axes at 45° towards the center of the MCP-PMT window. After leaving the 0.22 NA fibers the fluorescence pulses propagate 10 mm distance expanding to an approximate 6.3 mm diameter when reaching the 10 mm effective detector surface. An amplifier with 1.5 GHz bandwidth (Hamamatsu C5594) connected to the output of the MCP-PMT was used to amplify the signal before reaching the digitizer.

The synchronization of the optical and electronic signals is illustrated in Figure 3. TTL pulses, synchronized to the UV laser pulses, with 1 MHz repetition rate and 2 ns width were used to trigger a Stanford Research DG535 digital delay and pulse generator. This unit was customized to provide the 10–50 V pulse required to gate the MCP-PMT. The gate width was determined by the ~150 ns delay introduced between the shortest and longest fibers plus an allocation for the longest expected lifetime from the 629 nm channel (channel 4), resulting in a gate width of ~250 ns. However, the power dissipation capabilities of the internal 50 Ω MCP-PMT gate matching-impedance limited the gate pulse duty cycle to 1%. This meant that for the 250 ns gate width and 1% duty cycle a triggering frequency of 40 kHz was permissible. On the other hand, the pulse generator high voltage output was limited to pulses longer than 1 μs resulting in a gate triggering frequency of 10 kHz (i.e., 1% duty cycle).
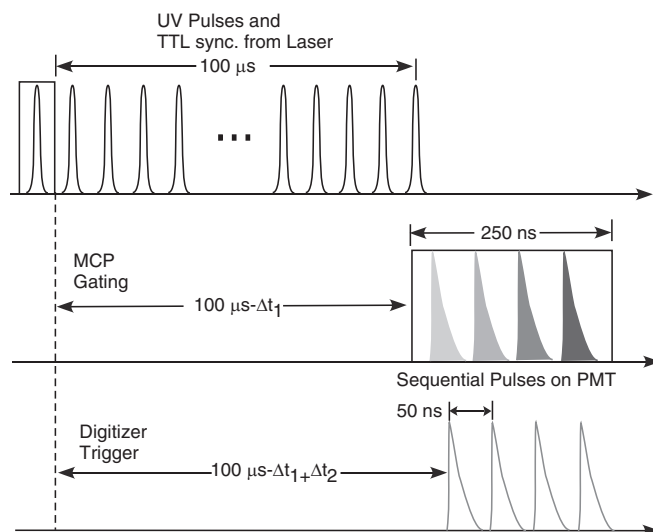

FIG. 2. Optical throughput of wavelength selection module.

FIG. 3. Timing diagram for ms-TRFS system. The delay time Δt_1 was adjusted to trigger the MCP-PMT before the arrival of the fluorescence pulse. The delay Δt_2 was adjusted to trigger the digitizer a few nanoseconds before the arrival of the MCP-PMT electrical signal pulses.

To time-resolve the fluorescence emission the electrical pulses from the MCP-PMT were recorded by a 3 GHz, 8 Gs/s, 10 bit digitizer (Agilent Acqiris U1065A-DC252) with 2.25 GHz analog bandwidth and 125 ps temporal resolution, which was also triggered by the pulse generator. The digitizer, in addition to its large memory size, high speed, and portability, includes processors and interfaces that enabled instrument control and rapid data transfer.

E. fTRFS system dispersion and fluorescence decay deconvolution

In the system described above the fluorescence pulse emission transients were affected by two factors: (1) the response time of the electronic components (MCP-PMT, amplifier and digitizer analog front-end) and (2) the use of multimode optical fibers for fluorescence collection which resulted in pulse broadening due the difference in group velocities between the modes traveling in the fiber, i.e., intermodal dispersion.[20] In a step index multimode fiber, where a very large number of modes propagate (in the fiber used in this work there were thousands of modes), the response time is given by the time difference between the fundamental mode and the highest order mode and is given by[20]

$$\tau_{mod} = \frac{n_1 L \Delta}{c_1}, \tag{1}$$

where $\Delta = (n_i - n_2)/n_1$, n_1 and n_2 are the index of refraction of the fiber core and cladding, respectively, L is the fiber length, and c_1 is the speed of light in fused silica. For 390–400 nm wavelengths the intermodal dispersion is $\tau_{mod} = 56 \times L$, where L is in meters and τ_{mod} is in picoseconds, resulting in 56, 560, 1024, and 1568 ps for the 1, 10, 19, and 28 m fibers, respectively. In addition, the 600 ps response time of the combined MCP-PMT detector and amplifier also contributed to fluorescence pulse broadening resulting in a combined response time given by

$$\tau = \sqrt{\tau_{mod}^2 + \tau_{det}^2}, \tag{2}$$

where τ_{det} is the detector broadening.

To compensate for fluorescence pulse transient distortion the instrument response of the ms-TRFS system was measured experimentally. Ideally, in order to measure the system fluorescence impulse response function (IRF) the sample is excited with an optical pulse with a duration as short as possible. In addition, since multimode dispersion is a function of wavelength, the excitation pulse must have wavelengths close to those detected by the instrument's optical channels. The fiber laser (30 ps pulse width) mentioned above meets the pulse duration criteria, but the emission at 355 nm does not meet the wavelength requirement. In order to measure at a longer wavelength, fluorescence pulses from a 1 mM concentration of the hemicyanine dye 2-(p-dimethylaminosotyryl)pyridylmethyl iodide (Sigma-Aldrich Corp. Cat. No. 280135), also known as 2-DASPI, were used following excitation by the 30 ps, 6 nJ pulses from the UV 355 nm fiber laser. When dissolved in ethanol, 2-DASPI has a very short (~30 ps) average lifetime and
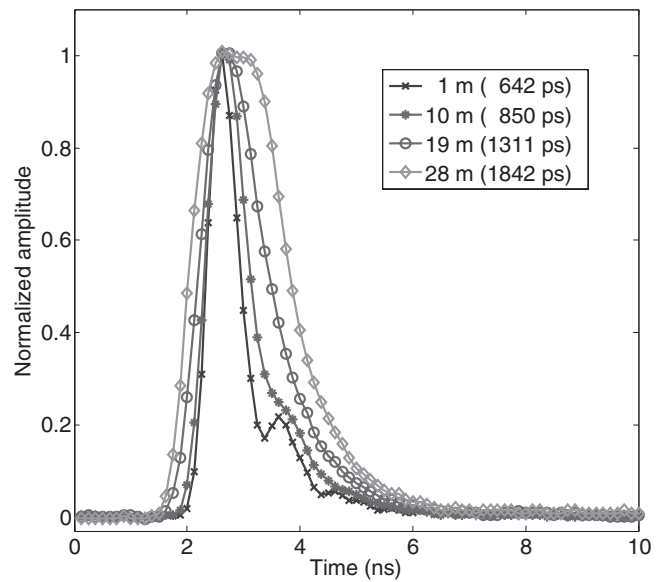

FIG. 4. Fluorescent pulses from 2-DASPI, excited by 355 nm, 30 ps, 6 nJ pulses. The multimodal dispersion resulted in ~300 ps progressive broadening of the fluorescent pulses.

emission spectrum with a maximum at approximately 550 nm,[21] which was better matched to the transmission spectra of the optical channels. Given than the excitation with the 2-DASPI was 15–20 times shorter than the detection system response time it was considered to be an impulse excitation that resulted in a direct measurement of the instrument response function. Since the emission spectra of 2-DASPI matched the detection window of the channel centered at 542 nm, successive measurements of fluorescence IRF were performed after connecting all different fiber lengths to this channel. Figure 4 depicts the measured dispersion introduced by the four multimode fiber lengths after connecting each fiber to channel 3 and after fluorescence pulse propagation through 1, 10, 19, and 28 m long multimode fibers.

For the 1 m fiber trace the system dispersion was dominated by the approximately ~600 ps temporal response of the MCP-PMT, amplifier, and excitation fiber dispersion. The longest instrument response was found for the 28 m fiber, at ~1800 ps. The secondary peak observed for the 1 m trace was attributed to an impedance mismatch between the MCP and the amplifier. The combination of the fiber dispersions calculated above with $\tau_{det} = 642$ ps (dispersion measured for the 1 m fiber, see Fig. 4) using Eq. (2) results in 692, 888, 1235, and 1713 ps, respectively. The discrepancies between these results and those of Fig. 3 may originate on the uncertainty of how the modes were actually populated in a multimode fiber.

With the instrument temporal response determined for all the instrument channels the measured time-resolved signal, $y(t)$, can be approximated by the convolution of impulse responses from the fluorescence IRF, $h(t)$ and the instrument temporal response, $I(t)$. In discrete time representation, for N equal sampling time points, $t_i = i\delta t$, for $i = 0, \ldots, N - 1$ and sampling time interval δt, we have

$$y(k) = \sum_{i=0}^{k} I(k - i)h(i) + \varepsilon_k, \tag{3}$$

where ε_k is the additive noise at time point t_k. To determine the fluorescence IRF, a non-parametric model based on Laguerre expansion of kernels and a constrained least-squares deconvolution algorithm was employed as previously reported in Ref. 22. In brief, the IRF was decomposed onto an ordered set of discrete time Laguerre functions (LFs), $b_l(k; \alpha)$ as

$$h(k) = \sum_{l=0}^{L-1} c_l b_l(k; \alpha), \tag{4}$$

where $l = 0, \ldots, L - 1$ is the order of LF and $0 \leq \alpha \leq 1$. The parameter, α, determined using the methodology presented in Ref. 22, dictates the rate of decay of the LF and c_l are the Laguerre expansion coefficients. In this work $L = 8$ was used and $\alpha = 0.8$ for Rose Bengal and 0.9 for all other dyes. The expansion coefficients were estimated and given by $\hat{c}_l$. The estimate for fluorescence decay profile followed from (4),

$$\hat{h}(k) = \sum_{l=0}^{L-1} \hat{c}_l b_l(k; \alpha). \tag{5}$$

Thus, the fluorescence system is fully characterized by the shape of its decay profile. In this study the average lifetime was computed as

$$\hat{\tau}_{\text{avg}} = \frac{\delta t \sum_{k=0}^{N-1} k \hat{h}(k)}{\sum_{k=0}^{N-1} \hat{h}(k)}. \tag{6}$$

III. SYSTEM VALIDATION

A. System validation in point-spectroscopy mode with fluorescent dyes and biomolecules

Organic dyes with well-known fluorescence lifetimes and emission spectra were used to determine whether correct fluorescence lifetimes could be retrieved from each optical channel independent of its fiber length. The organic dyes used where: Rose Bengal B (Sigma Aldrich CAS 11121-48-5), Coumarin 120 (Exciton Coumarin 440), Coumarin 1 (Exciton Coumarin 460) and Rhodamine B (Exciton Rhodamine 610) prepared at 100 μM concentration in ethanol. The fluorescence emission peaks vs full-width-half-maximum (FWHM) of these dyes are at about 573/34,[23] 440/60,[24] 460/60,[23] 565/40 nm,[23] respectively. The measured and fitted fluorescence signals along with the deconvolved fluorescent decay profiles from the organic dyes are presented in Figure 5. For all dyes with large SNR the fluorescent signal was measured from at least two channels (wavelength sub-bands). The lifetime measurements were performed acquiring 2000 sample temporal scans at 125 ps sampling interval, resulting in 250 ns scan duration. To improve the S/N ratio during acqusition averaging was performed over 32 subsequent scans. The MCP-PMT gain was set at 2100 V.

The average lifetimes of the organic dyes obtained from the intrinsic fluorescence decays after deconvolution of the instrumental response are listed in Table I.

Two major autofluorescent tissue constituents, i.e., structural proteins collagen and elastin, were used to determine the overall system ability to analyze the more complex fluorescence decays of these biomolecules. Measurements were

conducted using collagen type 1 from commercially available bovine Achilles tendon (Sigma Aldrich CAS 9007-34-5, dry powder) and commercially available elastin from bovine neck ligament (Sigma Aldrich CAS 9007-58-5, dry powder). Measurements were repeated 64 times each performed as indicated above with the exception that averaging was over 256 subsequent scans for each measurement. The fluorescence emission of these fluorophores was primarily observed in Channel 1 and Channel 2 of the ms-TRFS system. Table II depicts their average lifetimes obtained after deconvolution of the instrument response in comparison with values reported in the literature for similar experimental conditions (excitation wavelength, dry powder samples). This table also includes the range of values reported in the literature for Laguerre deconvolution which are limited to excitation wavelengths and dry powdered samples very similar to the ones used in this work.

B. Characterization of fluorescence lifetime measurement variability

The additive experimental noise (see Eq. (3)) introduced by the system components is likely to affect the fluorescence lifetime values of the measured samples. To study the effect of noise on the deconvolved lifetime values, five consecutive fluorescence measurements were performed under identical conditions for each fiber length; where each fiber was connected one-by-one to the same channel. Two organic dyes Rose Bengal and Rhodamine B (sub- and multi-nanosecond lifetime, respectively) were used to determine the lifetime measurement variability. The signal from the channel best matched to the dye peak emission spectrum (i.e., channels 4 and 3, respectively) resulting in the largest detected signal (best SNR), was used in the analysis. Data points were collected at 125 ps time interval in a 250 ns temporal window (2000 samples) and averaged over 32 data points. The experimental results are shown in Fig. 6 and summarized in Table III.

Rose Bengal presented the largest standard deviation (42 ps or $\sim$5% of mean) for the 10 m fiber. Identical means and a small difference in standard deviation and SNR were measured for the 10 and 28 m fibers. Also for this dye, the smallest standard deviation was 33 ps associated with one of the largest SNR (56 dB), which originated from the 19 m fiber. The largest difference in means was 60 ps measured between the 1 and 19 m fibers, while the largest difference between SNR's was 4.5 dB measured from the 10 and 28 m fibers. For Rhodamine B the largest standard deviation was 32 ps, or about $\sim$1% of mean, with SNR of 56.5 dB measured form the 28 m fiber. The smallest standard deviation was 19 ps with the largest SNR (59 dB) measured from the 1 m fiber. The largest difference in means was 310 ps measured between 1 and 28 m fibers, while the largest difference between SNR's was 2.5 dB measured from the 1 and 28 m fibers.

C. System validation in spectroscopic imaging mode or FLIm with fluorescent dyes

In order to evaluate the ms-TRFS ability to accurately record time-resolved fluorescence data during scanning, a set
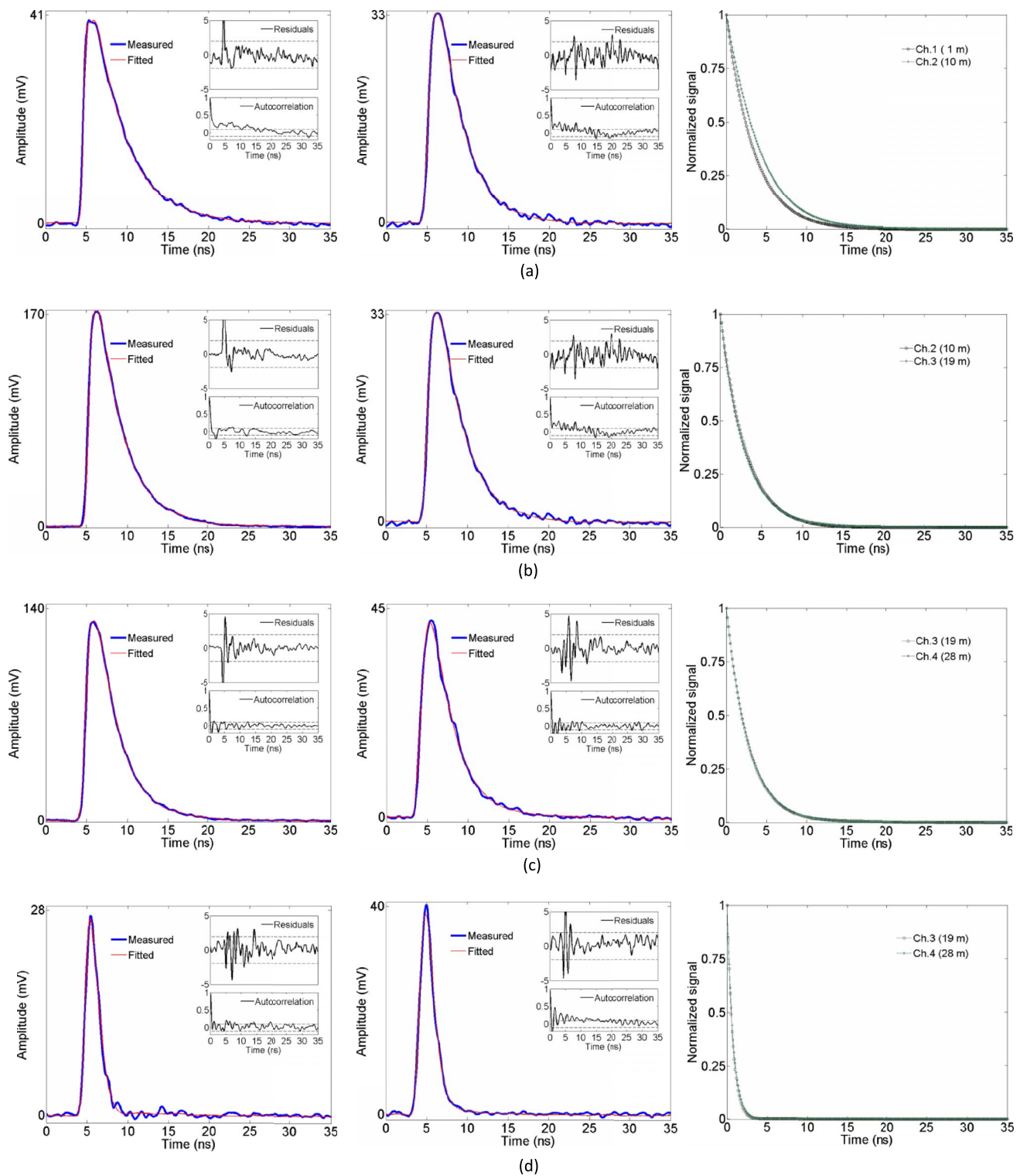
FIG. 5. From left to right: (a) Measured (M) and fitted (F) fluorescent signals for channels 1 and 2 and deconvolved fluorescent decay profile for Coumarin 120; (b) M and F fluorescent signals for channels 2 and 3 and deconvolved fluorescent decay profile for Coumarin 1; (c) M and F fluorescent signals for channels 3 and 4 and deconvolved fluorescent decay profile for Rhodamine B; (d) M and F fluorescent signals for channels 3 and 4 and deconvolved fluorescent decay profile for Rose Bengal. The insets show the corresponding normalized residuals and autocorrelation function.

of studies were conducted in fluorescence dyes placed in sealed borosilicate glass capillary tubes with 1.0 mm outer diameter and 0.78 mm inner diameter (Sutter Instruments BF100-78-10). Specifically, the capillaries were filled with organic dye solutions of Coumarin 120, Coumarin 1 and Rho-

damine B prepared in ethanol. The dye fluorescence width, listed in Sec. III A, span the wavelength of operation of at least two, and in the case of Coumarin 120 three, wavelength selection module optical channels. To obtain comparable signal levels from all optical channels without having to adjust

TABLE I. Lifetime measurements and values from the literature for the organic dyes used for system validation.

	Measured (ns)				Literature (ns)
	CH1	CH2	CH3	CH4	
Rose Bengal			0.85	0.87	0.739–0.820[25–28]
Coumarin 120	3.94	3.70			3.64–3.85[29]
Coumarin 1		3.22	3.42		3.1[30]

the MCP-PMT gain (1.94 kV), the concentration of Coumarin 120 was diluted to 30 μM while the concentration of the other two dyes was kept at 100 μM. The capillary tubes were mounted in parallel, 1 mm apart, on an anodized aluminum plate. Two dimensional scans of the area of interest were performed with the excitation/collection optical fiber of the ms-TRFS system mounted on an XY motorized stage (Aerotech MX80). In order to improve the system spatial resolution the 600 μm fiber used for the above point measurements was substituted with a 200 μm fiber. The tip of the optical fiber was set to a 200–300 μm distance with respect to the surface of the capillary tubes. Based on the fiber numerical aperture and the fiber-capillary distance the pump beam spot size at the surface of the capillaries was calculated to be approximately 300 μm.

Based on this spot size, and to keep a manageable data size, the scanned area was set to five 8 mm long lines separated by 0.5 mm pitch resulting in an X = 8 mm by Y = 2.5 mm image. The scanning stage speed was set to 10 mm/s along X and 50 mm/s along Y with an acceleration/deceleration of 500 mm/s^2. Data acquisition was performed at 5000 scans per second, total data length of 48 000 scans, and 2000 samples at 125 ps interval resulting in an image acquisition time of approximately 9.6 s. After averaging over 32 subsequent temporal scans the estimated time per pixel was 6.4 ms.

Due to the small volume of dye contained by the capillary tubes the fluorescence signal generated per laser pulse was small, therefore, to improve the S/N ratio, averaging was performed over 32 adjacent measurements. The fluorescent lifetime images (four spectral sub-bands as a function of spatial coordinated) obtained as described above are shown in Fig. 7 and histograms depicting the image lifetime measurement variability are shown in Fig. 8.

Consistent lifetime values were obtained for the fluorophores emitting in channels 1, 2, and 4. The largest variability of lifetime (Fig. 8) was observed for channel 3 where none of the fluorophores had a strong emission. The low SNR resulted in a broad distribution of the lifetime values. A comparison between the lifetimes obtained in the scanning mode experiments with those of Tables I and III (point measurements),

TABLE II. Lifetime measurements and values found in the literature for the biological compounds used for system validation.

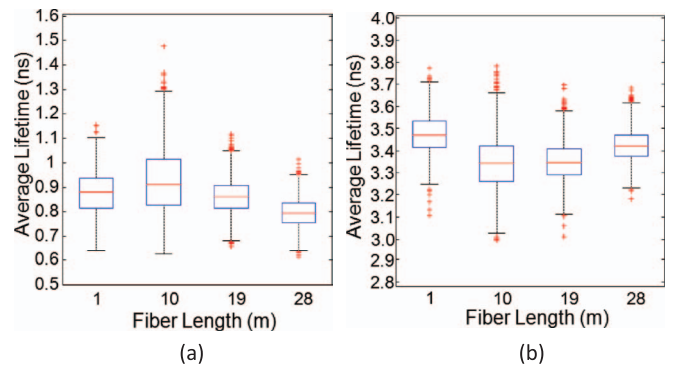|	CH1 (ns)	CH2 (ns)	Literature (ns)[1,31,32]
Collagen	5.30 ± 0.09	5.51 ± 0.08	1.42–5.30
Elastin	5.06 ± 0.05	5.51 ± 0.04	2.3–7.36

FIG. 6. Lifetime measurement variability for Rose Bengal (a) and Rhodamine B (b). The box edges for each fiber length represent the first and third quantile (q_1, q_3), respectively, where q_1 and q_3 are the 25th and 75th percentiles. The central mark represents the median. The whiskers extend from $q_1 - 1.5(q_3 - q_1)$ to $q_3 - 1.5(q_3 - q_1)$. The values outside the whisker extents (red "+") are considered outliers (beyond three standard deviations).

however, indicates very similar lifetime values for Rhodamine B, Coumarin 1, and Coumarin 120.

IV. DISCUSSION

In this study we developed a compact apparatus that enabled fast and robust multispectral time-resolved fluorescence spectroscopy measurements. Both fluorescence spectral intensities and spectrally resolved decay parameters can be obtained simultaneously in response to a single pulse light excitation. Unique to this fluorescence lifetime instrument is its ability to operate in multiple modes, i.e., point-spectroscopy, line-scanning, and planar XY-scanning; the latter mode of operation permits spectroscopic imaging, i.e., fluorescence lifetime imaging (FLIm). This is an important feature, as diverse tasks (based on the user needs) can be performed using a single instrument.

Practical applicability of such system, however, requires a rigorous evaluation of the optical throughput for all spectral channels, accurate measurement of the instrument response function (IRF) in each spectral channel, and study of the lifetime measurement variability as a function of experimental noise. The system presented in this work has been submitted to all these measurements and has proven to be stable and has been transported without loss of alignment or performance. In addition, due to its small footprint it can be easily integrated into rolling instrument carts or other systems.

TABLE III. Mean, standard deviation, and SNR after repeated measurement of the fluorescence lifetime of Rose Bengal and Rhodamine B.

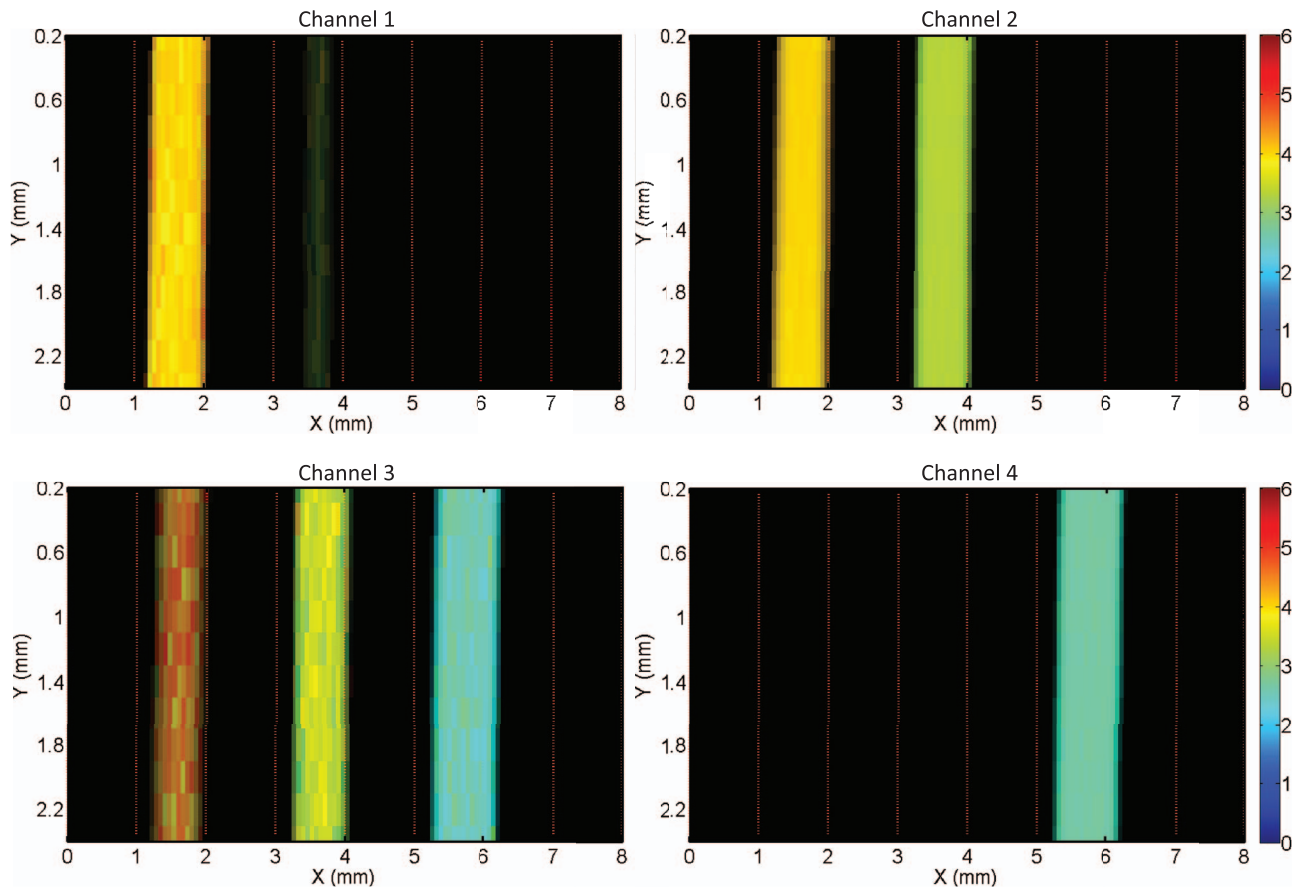|	Rose Bengal		Rhodamine B	
Fiber length (m)	Mean (ns)	SNR (dB)	Mean (ns)	SNR (dB)
1	0.81 ± 0.04	55.0	2.79 ± 0.02	59.0
10	0.82 ± 0.04	52.4	2.93 ± 0.03	57.8
19	0.87 ± 0.03	56.0	3.00 ± 0.03	58.3
28	0.82 ± 0.04	56.9	3.10 ± 0.03	56.5

FIG. 7. Lifetime images for 1.0 mm outer diameter and 0.78 mm inner diameter capillary tubes filled, from left to right, with Coumarin 120, Coumarin 1, and Rose Bengal. The color bar represents the measured lifetime in nanoseconds. The pixel size is 64 μm along X direction and 200 μm along Y direction. The typical width of the capillary tubes measured from the images is 12–15 pixels, equivalent to 0.768 mm – 0.96 mm.
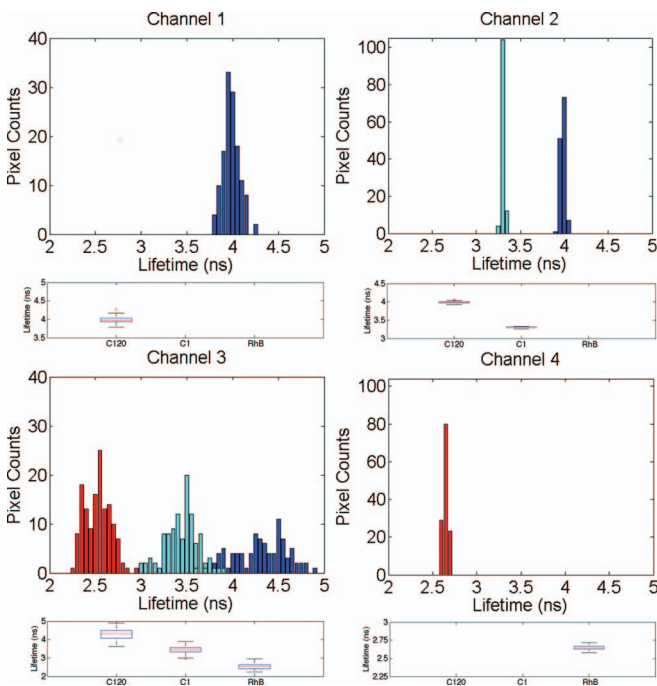

FIG. 8. Histograms and box-plots indicating the spectroscopic image lifetime measurement variability of the samples from Fig. 7 (red bars: Rhodamine B, cyan bars: Coumarin 1, blue bars: Coumarin 120). The statistical parameters used for the box-plots are identical to those of Fig. 6.

A. System spectral characteristics

For optimization of the overall fluorescence measurement, the ms-TRFS instrumentation requires a careful evaluation of the optical throughput as this varies from channel to channel, thus a spectral response function has to be generated for each optical channel if spectral intensities are used in characterization of fluorescent system (i.e., tissue). Moreover, decreased SNR is also known to affect the accurate recovery of the measured lifetime.[22] For this purpose, the optical filters and dichroic beamsplitters used in the wavelength selection module require a carefully selection for maximized transmittance, or reflectance depending on the component function. In current configuration, they exceed 90%. The multimode optical fibers and coupling lenses requires a good NA matching and, when possible, the lenses need to be coated with broadband anti-reflection coatings. In the present configuration (Figure 2) the optical throughput of Channels 1 and 2 transmit approximately 60% of the optical signal that falls within their spectral bandwidth, while Channels 3 and 4 transmit approximately 45% and 35%, respectively, resulting in spectral transmission ratios of 0.80:1.00:0.80:0.66. Thus, corrections to these coefficients need to be applied to compensate for the detector's wavelength dependent optical to electrical conversion efficiency. The optical losses were due in part to the collimated beam arriving from the 400 μm

fluorescence collection fiber that cannot be effectively coupled into the 200 μm delay fibers, small insertion losses introduced by the dichroic beamsplitters and minor beam clipping. In spite of an average channel throughput of approximately 50% the resultant system was highly efficient requiring less than 10 nJ per laser pulse for the detection of tissue autofluorescent components. As shown in Table III, signals with excellent SNR can be obtained for MCP-PMT gain voltages well below the allowed maximum (3.4 kV).

The wavelength selection module used in the current design has a modular construction that allows the straightforward expansion of optical (wavelength) channels or optimization of distinct spectral bandwidths (narrowing or broadening) based on the application. The current system was designed with an ability to resolve four key auto-fluorescent spectral bands from tissue that are sensitive to collagen, NADH, elastin, lipopigments, flavins, and porphyrins emissions. The laser delivery and fluorescence collection was executed through the same optical fiber providing a self-aligned fluorescence excitation and collection probe with a high optical efficiency. This enables the fluorescence excitation-collection via endoscopes or catheters including intravascular catheters which require small diameter.[33]

B. Data acquisition speed

Practical clinical implementation of ms-TRFS requires a fast data acquisition speed which can be limited by three factors: the laser repetition rate, the use of gated PMTs, and data storage capabilities.

The use of a high repetition rate diode-pumped mode-locked fiber-laser in current configuration provided a significant improvement in the speed of data acquisition (up to 1 MHz) when compared with earlier reported system that employed a Nitrogen laser operating at 30 Hz. While the use of a low repetition rate laser is still a viable source for point-spectroscopy measurements, this is impractical for a scanning or clinical FLIm implementation of the ms-TRFS. The use of a light source operating at high repetition rate (e.g., >10 KHz) would be essential for FLIm applications. Even though the Ytterbium fiber laser used in current study has two orders of magnitude lower energy per pulse than the nitrogen laser used in previous systems,[9] its five order of magnitude higher repetition rate results in a data acquisition rate increase of at least two orders of magnitude, which enables fast signal averaging for the rapid acquisition of fluorescent lifetime images. Less than 1 μs was required to record a data point from all four spectral channels and approximately 1 ms was required for the acquisition of one point when averaging is required to improve the S/N ratio. In addition, they offer improved pulse-to-pulse stability, require considerably less maintenance and the 355 nm laser wavelength is well matched to the absorption spectra of multiple endogenous fluorophores including collagen, NADH, flavins and porphyrins. However, the MHz laser pulse repetition rate from modelocked lasers can be excessive for many imaging applications. The very large amount of digital data that originates at high repetition rates can rapidly fill the mem-

ory of digitizers limiting the extension of scanned regions. This can be solved by using electro-optical modulators to reduce the excitation laser repetition rate. A possible alternative to the Ytterbium fiber lasers are high-speed Q-switched frequency tripled Nd:YAG lasers (355 nm) capable of μJ energy kHz pulses with less than 1 ns.[34,35] These lasers generate pulses with energy comparable to the nitrogen laser but with orders of magnitude larger repetition rate. However, their pulse-width is two orders of magnitude larger than mode-locked fiber lasers. Semiconductor lasers also have been applied to fluorescence spectroscopy is[5,8,36] but their pJ pulse energy and limited wavelengths of operation no shorter to 375 nm make them unsuitable for fluorescence spectroscopy applications in collagen.

The acquisition speed is not necessarily limited by the laser if gated photomultiplier detectors are used. The power dissipation capabilities of the MCP-PMT gate matching input impedance limits the trigger-pulse duty cycle to a few percent. This limitation, in combination to the ~1 μs pulse widths available from high voltage generators that drive the gate, restricts the triggering frequency to tens of kHz. This is still far less than the MHz pulse repetition rate provided by advanced laser systems such as the Ytterbium fiber laser discussed above. Thus, during data acquisition with gated detectors the vast majority of fluorescence pulses will not be detected and the sample may be unnecessarily exposed to high average laser power that might cause photobleaching.

C. System time-domain characteristics

The ability of the ms-TRFS to resolve the fluorescence decay is affected by both system components (electronics and optical delay fibers) and lifetime deconvolution method. The measured time-resolved fluorescent signal depends on the convolution of many bandwidths, including those of the signal, the MCP-PMT, pre-amplifiers, and digitizer amplifiers. Ideally, every electronic component in the electrical signal path needs to have a bandwidth greater than the 3-dB bandwidth of the signal, or, equivalently, an impulse response faster than the fastest part of the signal.[37] In addition, the length of coaxial transmission lines has to be kept at a minimum, especially if RG58 cable, which has an attenuation of 0.7 dB/m,[38] is used. In the present configuration, after taking into account the bandwidth of the MCP-PMT and all the components in the electrical signal path, a fluorescence pulse resembling a delta function will be broadening to approximately 500 ps, while a fluorescence pulse from NADH with 500 ps lifetime, which is one of the fastest biological fluorophores, will be broadened to approximately 700 ps. For a longer lifetime fluorphore such as collagen (~5.5 ns lifetime, see Table I) the electronic broadening will be negligible and intermodal dispersion will dominate. The results presented in Figure 4 show that for a 1 m fiber intermodal dispersion is negligible and broadening is mainly due to electrical effects, while the opposite takes place for the long 19 m optical fiber.

Whereas the electrical bandwidth is a measure of the highest sinusoidal frequency that can be digitized, the sample rate is the clock rate for the A/D conversion and if

insufficient it can render a large bandwidth as useless. For time domain signals the Nyquist criteria (sampling at twice as fast as the highest frequency) is insufficient to accurately reproduce a signal, instead, it is recommended that the sampling rate should be three to four times the digitizer's bandwidth.[39] Considering that the fluorescence lifetimes of biological tissue fluorophores are in the 0.5–10 ns range, the 125 ps sample interval (12.5 GS/s sample rate) of the digitizer used for this work is adequate, especially if the electrical form the MCP-PMT has been broadened by the amplifiers. In the present configuration, based on the above criteria, the shortest electrical pulse that can be accurately digitized is in the 400 ps range.

In this study, an improved deconvolution algorithm[22] was used that allows for fast and accurate processing of the digitized spectroscopic data and shown to compensate for physical distortion (broadening) of the measured fluorescence pulse transient. The fluorescence signal from an organic dye transmitted via different channels originates from the same singlet energy level transition. Thus the dye is expected to have the same fluorescence lifetime regardless of the optical channel and the deconvolution to compensate for the dispersion introduced by the different fiber lengths employed by each channel. Results from the different dyes used for system characterization (Figure 5) confirm that after deconvolution almost identical decay profiles can be obtained irrespective of the channel fiber length. The robustness of the deconvolution technique is underscored by the normalized residuals which fell within the confidence interval and the absence of autocorrelation structure. For a given dye, the lifetimes reported in Table I from fluorescence signals that span two channels differ by less than 5% and have values that fall within, or very near to, the range reported in the literature. In addition, the artifact introduced to the instrument response function by the amplifier used after the MCP, see trace for the 1 m fiber in Fig. 4, was compensated during deconvolution and did not had an impact on recovery of the fluorescence decay.

While the biological fluorophores used for system validation in Sec. III A cannot act as validation standards since multiple parameters contribute to the lifetime of a biological compound (e.g., excitation and detection wavelength, prolonged sample exposure to laser radiation, humidity, and age of sample), they have been broadly studied and reported in the literature.[1] In addition, the fluorescence of biological compounds has contributions from multiple fluorophores,[1,40,41] therefore, the 10% difference in the elastin lifetimes measured from two different channels can be expected. The measurements reported in Table II were similar to the ones reported in Refs. 1 and 32 and indicate that the system was sensitive enough to extract consistent lifetimes from organic compounds but discrepancies still exist with other studies.[31]

Throughout all the measurements of the system SNR (Sec. III B) the results for Rhodamine B were better than Rose Bengal's (see Table III). The statistics that govern the MCP-PMT are very similar to those of the conventional PMT[42] the $SNR = \sqrt{F}$, where F is the number of photons arriving to the photocathode. The quantum yield of Rhodamine B is 0.65[43] while that of Rose Bengal is 0.05,[44] therefore, for iden-

tical excitation conditions and detector gain, the larger signal from Rhodamine B yields a larger SNR and overall smaller standard deviations. Also with regard to Table III, as well as Fig. 6, the results indicate that even though the lifetimes of both dyes differ by a factor of three, and their quantum efficiencies by a factor of 13, the measured standard deviations were very small with a minimum of 19 ps and a maximum of 42 ps. The standard deviation relative to the sub-nanosecond lifetime of Rose Bengal was ∼5% indicating that sub-nanosecond lifetime biological fluorophores, such as NADH, can be well characterized. In the context of this work we acknowledge that the separabiltiy of multiple lifetime components has not been investigated and this can be affected by the system S/N ratio.

Previous experiments by Bec *et al.* have shown that the ms-TRFS is capable of acquiring two-dimensional lifetime image images from *ex vivo*[33] and *in vivo*[45] pig coronary arteries. The results has demonstrated that the instrument is sensitive to levels of fluorescence signal similar to that expected *in vivo* human arteries while *in vivo* result clearly shows the delineation between areas corresponding to arterial wall, catheter sheath and guide wire.

D. System imaging characteristics

The acquisition of high-resolution spectroscopic images required pixel capture with multimode fibers with small as possible diameter. For predetermined pulse excitation energies usually limited by the pump source capabilities, or the maximum permissible exposure[46] a tradeoff between resolution and SNR cannot be avoided. For this work, to obtain an optimum resolution, the spectroscopic imaging experiments performed in Sec. III C required a factor of three reduction in fiber diameter. In addition, a further decrease in SNR could be expected if averaging is reduced during data acquisition in order to expedite the image capture time while large averaging could have a detrimental effect on resolution. Thus, the scanning parameters of such system need to be optimized based on the application and imaging requirements.

V. CONCLUSIONS

This article reports the development and validation of a fiber-optic based compact configuration for simultaneous time- and wavelength-resolved fluorescence spectroscopy. The design solutions incorporated into the current prototype enhances its capabilities when compared with earlier prototypes using a similar principle. Current ms-TRFS apparatus has a small footprint and a modular design that allows for customization of spectral bands (or channel) as needed. The use of a diode-pumped modelocked fiber laser along with an advanced digitizer technology enabled fast signal averaging and data acquisition speed. Multispectral acquisition/storage of one point measurement with excellent S/N ratio required approximately 6.4 ms, while acquisition of a 1500 pixel image required approximately 9.6 s. The fiber laser at 355 nm wavelength is also a better matched to the absorption spectra of collagen cross-links, NADH, flavins,

and porphyrins. The new system was found to be highly efficient requiring less than 10 nJ of laser pulse energy for the detection of tissue autofluorescent components and required a few milliseconds for the acquisition of one point measurement.

The optimized non-parametric method (Laguerre expansion technique) used for the deconvolution of fluorescent decay allowed for a robust recovery of the fluorescence impulse response function for each spectral channel despite the differential pulse broadening in these channels. The validation of the system performed with a variety of organic dyes that span the wavelength of operation of all optical channels has demonstrated that for all channels the measured fluorescent lifetimes values were robustly recovered. Also, the lifetimes values determined from compounds with fluorescent bandwidth that spans at least two optical channels (each with multimode fibers that vary in length by ten meters) differed by less than 10%. This indicates that multimode dispersion effects introduced by the long multi-mode fibers were properly compensated by the deconvolution algorithm. The system validation performed with biological compounds (collagen and elastin) underscored the findings from organic dyes. Experiments assessing the lifetime measurement variability due to large variations in fluorophores lifetime and quantum efficiency demonstrated that the ms-TRFS was a sensitive and precise system capable of extracting consistent lifetimes from organic compounds.

The ms-TRFS high optical throughput and rapid point acquisition time allows the straightforward integration with two-dimensional, or rotary,[33] high-resolution spectroscopic imaging configurations. The 200 μm diameter fluorescent detection fiber used for two-dimensional image acquisition resulted in 300 μm pixel image size and approximately 9 s were required to obtain a 8×2.5 mm image. Moreover, the lifetimes measured during imaging experiments were very similar to those obtained by point-spectroscopic acquisition using a 600 μm fiber diameter.

In addition, this article presents a set of technical validation procedures and steps important to address in the development of similar ms-TRFS or FLIm devices. Spectral calibration and pulse distortion along with system response and experimental noise in each spectral channel are expected to play role in accurate intensity calibration and recovery of fluorescence lifetimes, respectively.

In summary, the ms-TRFS system has proven to be suitable for fast, accurate and precise lifetime measurement of low quantum efficiency sub-nanosecond lifetime fluorophores. Notable is this system versatility. The ms-TRFS not only can operate in both point-spectroscopy mode and scanning spectroscopic imaging mode, but also enable measurements of a broad range of fluorescence lifetimes simultaneously in multiple spectral channels.

ACKNOWLEDGMENTS

[1]J. M. I. Maarek, L. Marcu, W. J. Snyder, and W. S. Grundfest, Photochem. Photobiol. **71**(2), 178–187 (2000).

[2]L. Marcu, Ann. Biomed. Eng. **40**(2), 304–331 (2012).

[3]T. J. Pfefer, D. Y. Paithankar, J. M. Poneros, K. T. Schomacker, and N. S. Nishioka, Lasers Surg. Med. **32**(1), 10–16 (2003).

[4]M.-A. P. B. W. Mycek, *Handbook of Biomedical Fluorescence* (Marcel Dekker, New York, 2003).

[5]D. Schweitzer, M. Hammer, F. Schweitzer, R. Anders, T. Doebbecke, S. Schenke, and E. R. Gaillard, J. Biomed. Opt. **9**(6), 1214–1222 (2004).

[6]L. Marcu, M. C. Fishbein, J.-M. I. Maarek, and W. S. Grundfest, Arteriorscler., Thromb., Vasc. Biol. **21**(7), 1244–1250 (2001).

[7]R. A. Schwarz, W. Gao, C. Redden Weber, C. Kurachi, J. J. Lee, A. K. El-Naggar, R. Richards-Kortum, and A. M. Gillenwater, Cancer **115**(8), 1669–1679 (2009).

[8]W. R. Lloyd, R. H. Wilson, C. W. Chang, G. D. Gillispie, and M. A. Mycek, Biomed. Opt. Express **1**(2), 574–586 (2010).

[9]Y. Sun, R. Liu, D. S. Elson, C. W. Hollars, J. A. Jo, J. Park, Y. Sun, and L. Marcu, Opt. Lett. **33**(6), 630–632 (2008).

[10]W. Becker, A. W. Castleman, J. P. Toennies, and W. Zinth, "The bh TCSPC Handbook" (Springer Verlag, Berlin, 2005).

[11]S. Kumar, C. Dunsby, P. A. A. De Beule, D. M. Owen, U. Anand, P. M. P. Lanigan, R. K. P. Benninger, D. M. Davis, M. A. A. Neil, P. Anand, C. Benham, A. Naylor, and P. M. W. French, Opt. Express **15**(20), 12548–12561 (2007).

[12]J. McGinty, N. P. Galletly, C. Dunsby, I. Munro, D. S. Elson, J. Requejo-Isidro, P. Cohen, R. Ahmad, A. Forsyth, A. V. Thillainayagam, M. A. A. Neil, P. M. W. French, and G. W. Stamp, Biomed. Opt. Express **1**(2), 627–640 (2010).

[13]J. Phipps, Y. Sun, R. Saroufeem, N. Hatami, M. C. Fishbein, and L. Marcu, J. Biomed. Opt. **16**(9), 096018–096018 (2011).

[14]P. V. Butte, Q. Y. Fang, J. A. Jo, W. H. Yong, B. K. Pikul, K. L. Black, and L. Marcu, J. Biomed. Opt. **15**(2), 027008 (2010).

[15]A. Ruck, C. Hulshoff, I. Kinzler, W. Becker, and R. Steiner, Microsc. Res. Tech. **70**(5), 485–492 (2007).

[16]R. Erdmann, *Time Correlated Single-Photon Counting and Fluorescence Spectroscopy* (Wiley-VCH, Weinheim, 2005).

[17]Y. H. Sun, Y. Sun, D. Stephens, H. T. Xie, J. Phipps, R. Saroufeem, J. Southard, D. S. Elson, and L. Marcu, Opt. Express **19**(5), 3890–3901 (2011).

[18]V. Y. Soloviev, K. B. Tahir, J. McGinty, D. S. Elson, M. A. A. Neil, P. M. W. French, and S. R. Arridge, Appl. Opt. **46**(30), 7384–7391 (2007).

[19]Y. H. Sun, N. Hatami, M. Yee, J. Phipps, D. S. Elson, F. Gorin, R. J. Schrot, and L. Marcu, J. Biomed. Opt. **15**(5), 056022 (2010).

[20]G. Keiser, *Optical Fiber Communications* (McGraw Hill, New York, NY, 1983).

[21]J. Kim, M. Lee, J. H. Yang, and J. H. Choy, J. Phys. Chem. A **104**(7), 1388–1392 (2000).

[22]J. Liu, Y. Sun, J. Y. Qi, and L. Marcu, Phys. Med. Biol. **57**(4), 843–865 (2012).

[23]S. Prahl, PhotochemCAD, Rose Bengal Fluorescence Spectra (Oregon Medical Laser Center, 2012).

[24]C. Eastman Kodak, *Kodak Optical Products* (Eastman Kodak Company, 1991).

[25]J. R. Lakowicz, *Principles of Fluorescence Spectroscopy* (Kluwer, New York, 1999).

[26]G. R. Fleming, A. W. E. Knight, J. M. Morris, R. J. S. Morrison, and G. W. Robinson, J. Am. Chem. Soc. **99**(13), 4306–4311 (1977).

[27]H. E. Zimmerman, J. H. Penn, and C. W. Carpenter, *Proc. Natl. Acad. Sci. U.S.A.* **79**(6), 2128–2132 (1982).

[28]L. E. Cramer and K. G. Spears, J. Am. Chem. Soc. **100**(1), 221–227 (1978).

[29]H. Pal, S. Nad, and M. Kumbhakar, J. Chem. Phys. **119**(1), 443–452 (2003).

[30]G. Jones, W. R. Jackson, C. Choi, and W. R. Bergmark, J. Phys. Chem. **89**(2), 294–300 (1985).

[31]A. S. Dabir, C. A. Trivedi, Y. Ryu, P. Pande, and J. A. Jo, J. Biomed. Opt. **14**(2), 024030 (2009).

[32]A. Zukauskas, P. Vitta, N. Kurilcik, S. Jursenas, and E. Bakiene, Opt. Mater. **30**(5), 800–805 (2008).

[33]J. Bec, H. Xie, D. R. Yankelevich, F. Zhou, Y. Sun, N. Ghata, R. Aldredge, and L. Marcu, J. Biomed. Opt. **17**(10), 106012 (2012).

[34]Short Laser Pulses at High Rep-Rate, Technical Note (Advanced Optical Technology Ltd., 2009).

[35]S. N. Cheng, J. J. Rico-Jimenez, J. Jabbour, B. Malik, K. C. Maitland, J. Wright, Y. S. L. Cheng, and J. A. Jo, Opt. Lett. **38**(9), 1515–1517 (2013).

[36]D. Schweitzer, S. Schenke, M. Hammer, F. Schweitzer, S. Jentsch, E. Birckner, W. Becker, and A. Bergmann, Microsc. Res. Tech. **70**(5), 410–419 (2007).

[37]"Insights into High-Speed Detectors and High-Frequency Techniques," New Focus Application Note#1 (Newport Corporation, 2013).

[38]See http://rfelektronik.se/manuals/Datasheets/Coaxial_Cable_Attenuation_Chart.pdf.

[39]"Digitizer/Oscilloscope Fundamentals," National Instruments, 14 November 2013. See http://www.ni.com/white-paper/3408/en/.

[40]E. Fujimori, Biochim. Biophys. Acta **828**(1), 104–106 (1985).

[41]D. Fujimoto, K. Y. Akiba, and N. Nakamura, Biochem. Biophys. Res. Commun. **76**(4), 1124–1129 (1977).

[42]S. Donati, *Photodetectors: Devices, Circuits, and Applications* (Prentice Hall PTR, Upper Saddle River, NJ, 2000).

[43]R. F. Kubin and A. N. Fletcher, J. Lumin. **27**(4), 455–462 (1982).

[44]S. M. Linden and D. C. Neckers, Photochem. Photobiol. **47**(4), 543–550 (1988).

[45]J. Bec, D. M. Ma, D. R. Yankelevich, J. Liu, W. T. Ferrier, J. Southard, and L. Marcu, "Multispectral fluorescence lifetime imaging system for intravascular diagnostics with ultrasound guidance: *in vivo* validation in swine arteries," J. Biophotonics (published online).

[46]American National Standards Institute, *American National Standard for Safe Use of Lasers in Health Care ANSI Z136.1* (Laser Institute of America, Orlando, FL, 2007).